



Contents lists available at ScienceDirect

Materials Science in Semiconductor Processing

journal homepage: www.elsevier.com/locate/mssp

Indium tin oxide etch characteristics using $C_xH_{2x+2}(x=1,2,3)/Ar$

Jong Woo Hong^a, Hyun Min Cho^c, Yu Gwang Jeong^c, Da Woon Jung^c, Yun Jong Yeo^c,
Ji Eun Kang^a, Hee Ju Kim^a, Hyun Woo Tak^a, Geun Young Yeom^{a,b,**}, Dong Woo Kim^{a,*}

^a School of Advanced Materials Science and Engineering, Sungkyunkwan University (SKKU), Suwon, Gyeonggi-do, 16419, Republic of Korea

^b SKKU Advanced Institute of Nanotechnology (SAINT), Sungkyunkwan University (SKKU), Suwon, Gyeonggi-do, 16419, Republic of Korea

^c Process Research Team, Samsung Display, 1, Samsung-ro, Giheung-gu, Yongin-si, 17113, Republic of Korea

ARTICLE INFO

Keywords:

ITO
Dry etching
Hydrocarbon
CH₄
C₂H₆
C₃H₈
Dry chamber cleaning

ABSTRACT

For the next generation display devices, dry etching technique for indium tin oxide (ITO) used as a transparent electrode is required to obtain a highly anisotropic etch profile, and to decrease the dimensional loss after the etching. For the dry etching of ITO, the easy dry cleaning of etch byproducts attached to the chamber wall during the dry etching is also important. In this study, by using novel hydrocarbon gases mixed with Ar, such as ethane (C₂H₆) and propane (C₃H₈), the dry etch characteristics and the etch residue cleaning process have been investigated using an inductively coupled plasma etcher, and the results were compared with the conventionally investigated methane (CH₄)-based gases, such as CH₄ and CH₄/H₂ mixed with Ar. The result showed that the hydrogen in CH₄/H₂ both decreased the ITO etch rate, and decreased the etch selectivity over photoresist (PR). By using hydrogen-less hydrocarbon gas having the alkane structure, such as C_xH_{2x+2} (x = 2, 3), both the ITO etch rate and the etch selectivity were increased with the increase of carbon in the alkane structure; therefore, the highest etch rate was observed for C₃H₈. In addition, with the increase of x in the carbon of C_xH_{2x+2}, less dimensional loss, more anisotropic etch profile, and lower surface roughness could be observed. During the etching, etch residues containing C, In, Sn, O, and H were accumulated on the chamber wall due to the low volatility of the etch byproducts; however, the etch residues formed by all three hydrocarbon gases could be successfully dry cleaned using H₂/Ar plasmas through the formation of InC_xH_y (x < y), CO_x, and S_nH_x.

1. Introduction

Indium tin oxide (ITO) is a material that is widely used in displays and optoelectronic devices because it is transparent and conducts electricity well [1–3]. To make ITO devices, etching, deposition, etc. are used. In particular, etching is one of the important processes, as it greatly affects the properties of ITO [4,5]. Currently, wet etching is used to pattern the ITO. The wet etching has a fast etch rate, low cost, and is easy to implement, but the etch profile is isotropic, and the dimensional loss is high [6–9]. Therefore, the wet etching method cannot be applicable to the ITO conductor lines with very narrow widths required for the next generation display devices.

Dry etching can provide an improved etch profile with less dimensional loss than wet etching [10–12]. To dry etch ITO, various gases, such as CH₄/H₂, BCl₃/Cl₂, CH₄/Cl₂, and HBr mixed with Ar, have been

investigated [13]. However, for halogen-based gases, that is, BCl₃/Cl₂, CH₄/Cl₂, and HBr mixed with Ar, although the ITO etched with halogen-based gases showed a clean etched sidewall surface, a high degree of contamination was observed on the chamber wall, while the etch selectivity over photoresist was not sufficiently high, due to the low volatility of indium halides, such as InCl_x and InBr_x [14,15]. Therefore, the etching was also performed with hydrogen-based gases, such as CH₄ and CH₄/H₂ mixed with Ar, to improve the ITO etch characteristics by forming possibly volatile etch products, such as In(CH₃)₂, etc. [16–18]. However, these gas chemistries showed lower etch rates and the etch profile was not sufficiently anisotropic for the application to next generation display devices; in addition, no information on the etch residue formed on the chamber wall and its cleaning method was offered [19].

In this study, to improve the ITO etch characteristics, the effects of novel hydrocarbon gases having the alkane structure (C_xH_{2x+2}), such as

* Corresponding author.

** Corresponding author. School of Advanced Materials Science and Engineering, Sungkyunkwan University (SKKU), Suwon, Gyeonggi-do, 16419, Republic of Korea.

E-mail addresses: gyyeom@skku.edu (G.Y. Yeom), dwkim111@gmail.com (D.W. Kim).

<https://doi.org/10.1016/j.mssp.2023.107395>

Received 2 January 2023; Received in revised form 10 February 2023; Accepted 11 February 2023

Available online 21 February 2023

1369-8001/© 2023 Elsevier Ltd. All rights reserved.

C_2H_6 and C_3H_8 , on the properties of etching were investigated; in addition, CH_4 using an inductively coupled plasma (ICP) etcher and their etch mechanisms were investigated. Further, the etch byproducts attached to the chamber wall during the etching using hydrocarbon gases were analyzed, and the method of *in situ* dry cleaning of those etch residues using the same ICP etcher were also investigated [20–22].

2. Experimental

The ITO etching was carried out using an ICP etching system. The ICP source was composed of external inner/outer two-turn copper coils coated with silver and a 35 mm thick alumina window on the top side of the reactor (see Fig. 9 (a)). The size of the substrate was 300 mm diameter, and it was made of anodized aluminum. The substrate was located 150 mm below the dielectric window. The chamber wall was also made of anodized aluminum and the chamber wall was kept at room temperature during the etching and cleaning. The ICP source was powered by 13.56 MHz rf power (Seren-R3001), and the substrate was biased by 12.56 MHz rf power (rf power amplifier, ENI - Model A1000RF). The process gas was uniformly sprayed through the gas ring located near the chamber top edge. The process pressure was adjusted automatically using a main valve (VAT-model PM.7) connected to a turbopump and a dry pump.

To etch ITO, 180 nm thick ITO thin film samples deposited on the glass substrate and masked with 3 μ m width PR were used. During the ITO etching, the substrate temperature was fixed at 70 °C, and the process pressure was kept at 2 mTorr. Hydrocarbon gases having the alkane structure of (C_xH_{2x+2}), such as CH_4 , C_2H_6 , and C_3H_8 mixed with Ar, were used for etching, and 2 kW of the ICP source power and -150 V of bias voltage were used.

To investigate the chamber wall dry cleaning contaminated during the ITO etching, 10 μ m bare ITO on 300 mm diameter glass substrate was continuously etched, and the etch residues were observed with the silicon wafer attached to the chamber wall. To dry clean the etch residues on the chamber wall, O_2 or H_2 mixed with Ar were used at the pressure of (30–90) mTorr while operating 2 kW of ICP source power only.

To measure the ITO etch rate, deposited residue thickness, and residue cleaning rate, a step profilometer (Tencor, Alpha step 500) was used. Scanning electron microscopy (FE–SEM; Hitachi, S-4700) was used to observe the profile after the etching of the PR masked ITO, and to measure the etch selectivity between the ITO and PR. The radicals of hydrocarbon gases dissociated by the plasma were observed through optical emission spectroscopy (OES; ANDOR technology, SR-ASZ-0103). In addition, quadrupole mass spectrometry (QMS; Hiden Analytical, PSM 500) was also used to observe the dissociated radicals and ionized species in the hydrocarbon plasmas. The composition of the etch byproducts on silicon wafers attached to the chamber wall was measured using X-ray photoelectron spectroscopy (XPS; VG Microtech Inc., ESCA2000). *In situ* deposition and cleaning of the etch residue on the sidewall of the chamber during ITO etching and cleaning were observed using a quartz crystal microbalance (QCM) installed on the chamber sidewall.

3. Results and discussion

3.1. Etching of ITO using C_xH_{2x+2} ($x = 1, 2, 3$)/Ar

Fig. 1 shows the ITO etch rate, PR etch rate, and ITO etch selectivity over PR measured as a function of H_2 percentage in CH_4/H_2 mixed with Ar. A fixed ratio of CH_4 : Ar of (2:1) was used, while adding H_2 to change the H_2 percentage; 2000 W of ICP source power and -150 V of bias voltage were applied, while maintaining the operating pressure at 2 mTorr and the substrate temperature at 70 °C. Fig. 1 shows that the increase in H_2 percentage in the CH_4/H_2 mixed with Ar increased the PR etch rate while not significantly changing the ITO etch rate up to 40% of

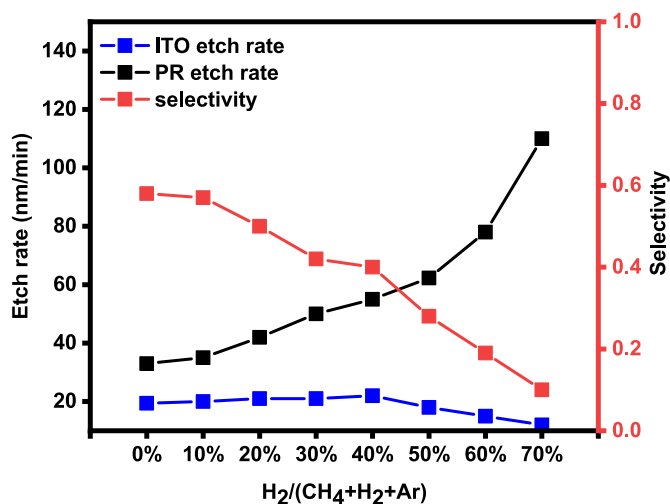


Fig. 1. Etch rates of ITO and PR, and their etch selectivity as a function of H_2 percentage in CH_4/H_2 mixed with Ar.

H_2 , and decreasing the etch rate by increasing the H_2 percentage further. So, the ITO etch selectivity was decreased from (0.6–0.1) with the increase of H_2 percentage from (0–70) %. In addition, the addition of H_2 to CH_4 generally increased the roughness of PR surface, possibly due to the micromasking of etch byproduct on the PR surface while etching the PR with hydrogen, as shown in Fig. S1 of the Supplementary Information (SI).

To decrease the effect of hydrogen on the ITO etching, the hydrocarbon gases mixed with Ar having the alkane structure of C_xH_{2x+2} , such as C_2H_6 and C_3H_8 , were used, in addition to CH_4 in the ITO etching, and their characteristics of ITO etching were studied. Fig. 2 shows the etch rates of ITO and the etch selectivity over PR measured as a function of Ar percentage in the C_xH_{2x+2}/Ar gas mixture. No hydrogen gas was added to the gas mixture, and the process conditions are the same as those in Fig. 1. The etch rates of ITO were increased with increasing Ar percentage in the C_xH_{2x+2}/Ar up to 90% of Ar percentage, while the further increase of Ar percentage decreased the etch rate. In contrast, the increase of Ar percentage in the gas mixture continuously decreased the etch selectivity over PR; however, the etch selectivity was generally higher than 1.0, except for CH_4/Ar . Comparison between the different hydrogen carbon gases showed that the etch rate and etch selectivity

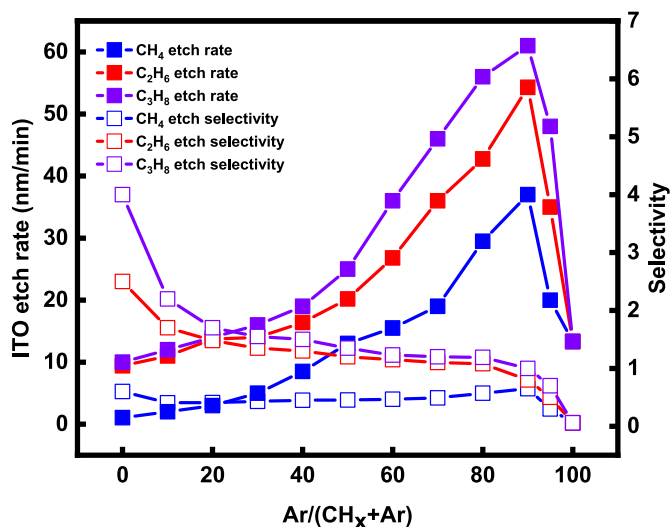


Fig. 2. Etch rates of ITO and PR, and their etch selectivity as a function of Ar percentage in C_xH_{2x+2} ($x = 1, 2, 3$) mixed with Ar.

were higher in the order: $\text{CH}_4 > \text{C}_2\text{H}_6 > \text{C}_3\text{H}_8$; therefore, the higher C/H ratio in the $\text{C}_x\text{H}_{2x+2}/\text{Ar}$ gas mixture increased both the etch rate and the etch selectivity over PR at the same Ar percentage.

The 180 nm thick ITO masked with 3 μm width PR was 30% over-etched with the condition of 50% Ar in the $\text{C}_x\text{H}_{2x+2}/\text{Ar}$ gas mixtures of Fig. 2, and the dimensional loss of the ITO line width after the over-etching was observed from the top of the etched ITO line using SEM, with the results shown in Fig. 3. After 30% ITO over-etching, the dimensional loss of ITO line width was decreased from (321.5–111) nm (CH_4 to C_3H_8) by using a hydrocarbon gas with a higher C/H ratio, due to the increased etch selectivity in the order: $\text{CH}_4 > \text{C}_2\text{H}_6 > \text{C}_3\text{H}_8$.

Fig. 4 shows the cross-sectional SEM images of the 3 μm width/1.5 μm thick reference PR on 180 nm thick ITO and the ITO lines after full etching of the 180 nm ITO with the condition of 50% Ar in the $\text{C}_x\text{H}_{2x+2}/\text{Ar}$ gas mixtures of Fig. 2, (a) reference and before the PR removal, and (b) after the PR removal. As shown in Fig. 4 (a), rougher PR surface was observed in the order: $\text{C}_3\text{H}_8 > \text{C}_2\text{H}_6 > \text{CH}_4$, that is, with decreasing C/H ratio in the $\text{C}_x\text{H}_{2x+2}/\text{Ar}$ gas mixture, possibly due to the micromasking by etch byproduct on the PR surface by etch byproducts, as mentioned earlier. And the etch selectivity was ~ 0.67 for CH_4 , ~ 1.07 for C_2H_6 , and ~ 1.67 for C_3H_8 . Fig. 4 (b) shows the etch slope width of ITO lines, that is, the etch profile angles after the etching. The etch slope width for CH_4 , C_2H_6 , and C_3H_8 was (135, 79, and 32) nm, respectively; therefore, the more anisotropic ITO etch profile was observed at the higher C/H ratio of the $\text{C}_x\text{H}_{2x+2}/\text{Ar}$ gas mixtures, in addition to smoother PR profile. Tilted SEM images of the PR-masked ITO after etching CH_4 , C_2H_6 , and C_3H_8 mixed with 50% H_2 are shown in Fig. S2 of the SI.

Fig. 5 shows the AFM data measured for the 180 nm thick ITO deposited on glass substrate (reference), and those etched about 150 nm thick ITO and 30% over-etched to expose the glass substrate with $\text{C}_x\text{H}_{2x+2}/50\%$ Ar gas mixtures for the etch conditions in Fig. 3.

Compared to the RMS surface roughness of the reference ITO, the RMS surface roughness of the ITO surfaces etched ~ 150 nm, and that of exposed glass substrate after 30% over-etching of ITO, were lower. Also, the RMS roughness values of the 150 nm thick etched ITO surface and exposed glass substrate surface by 30% over-etching were lower for the higher C/H ratio in the hydrocarbon gas. The etching with $\text{C}_x\text{H}_{2x+2}/\text{Ar}$ gas mixtures with higher C/H ratio appears to smooth the ITO surface, possibly by physical sputter etching indium and tin compounds formed on the ITO surface during the etching.

To understand the ITO etch mechanism with the $\text{C}_x\text{H}_{2x+2}/\text{Ar}$ gas mixtures, the dissociated species in the plasma were analyzed by OES and QMS. Fig. 6 shows the OES data observed with the plasmas generated with $\text{C}_x\text{H}_{2x+2}$ ($x = 1, 2, 3$) mixed with 50% Ar. As shown in Fig. 6 (a), variously dissociated peaks, such as CH [23], OH [24], C [23], and H [25], could be observed. Fig. 6 (b) shows that when the CH and H intensities normalized by Ar intensity were measured, even though the normalized CH intensity was increased with the increase of C/H ratio in the hydrocarbon gas mixture, the normalized H intensity did not noticeably vary with the C/H ratio in the hydrocarbon gas mixture. Therefore, as shown in Fig. 6 (c), the ratio of CH/H increased in the order: $\text{CH}_4 > \text{C}_2\text{H}_6 > \text{C}_3\text{H}_8$, indicating the importance of dissociated CH in the etching of ITO.

More accurate dissociated species in the plasma with the $\text{C}_x\text{H}_{2x+2}/\text{Ar}$ gas mixtures could be observed with QMS, and the QMS data are shown in Fig. 7 (a) and (c) for the radical mode, and (b) and (d) for the positive ion mode for $\text{C}_x\text{H}_{2x+2}$ ($x = 1, 2, 3$) mixed with 50% Ar. In the case of radical mode, the dissociated radicals in the plasma are ionized in the QMS, and their masses are detected by the analyzer; while in the case of positive ion mode, the positive ions in the plasma collected at the QMS are directly measured by the analyzer without further ionization; therefore, more accurate measurement of the dissociated species in the

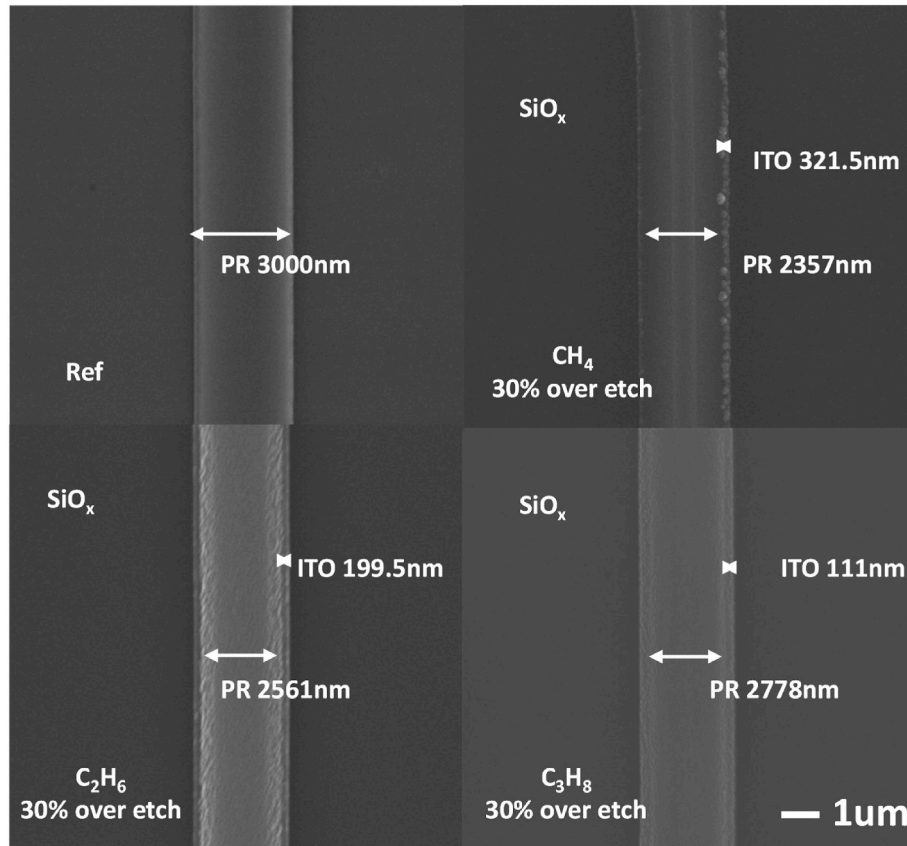


Fig. 3. Top SEM images of the 3 μm width reference PR-masked 180 nm thick ITO and the PR-masked ITO lines after 30% over-etching with $\text{C}_x\text{H}_{2x+2}/50\%$ Ar gas mixtures of Fig. 2.

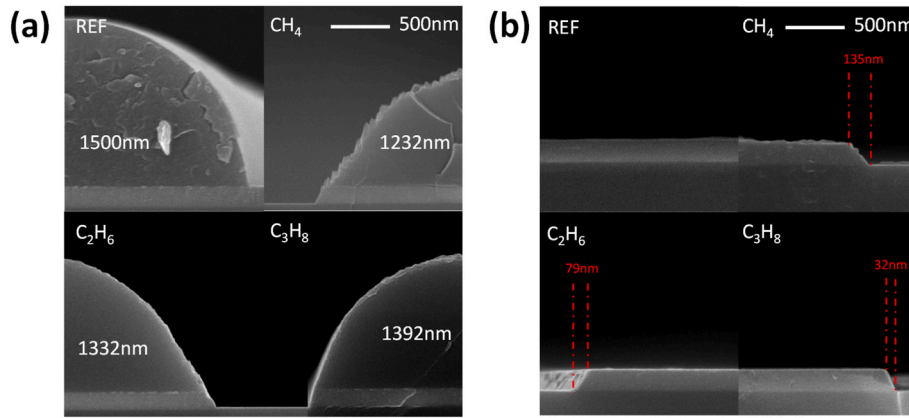


Fig. 4. Cross-sectional SEM images of the 3000 nm width/1500 nm thick reference PR on 180nm thick ITO and the ITO lines after full etching of 180 nm ITO with the condition of 50% Ar in the C_xH_{2x+2}/Ar gas mixtures of Fig. 2 (a) before PR removal, and (b) after PR removal.

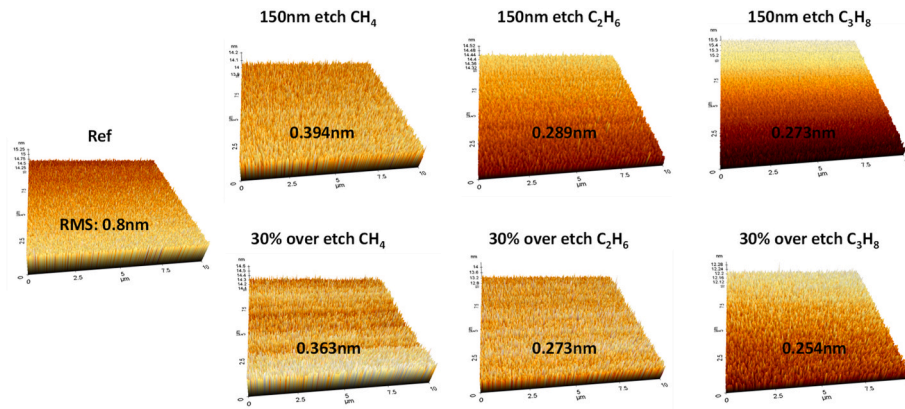


Fig. 5. Schematic of the RMS surface roughness of ITO/glass observed for 180 nm thick ITO reference, and those etched about 150 nm thick ITO and 30% over-etched (glass substrate) with $C_xH_{2x+2}/50\%$ Ar gas mixtures for the etch conditions in Fig. 3.

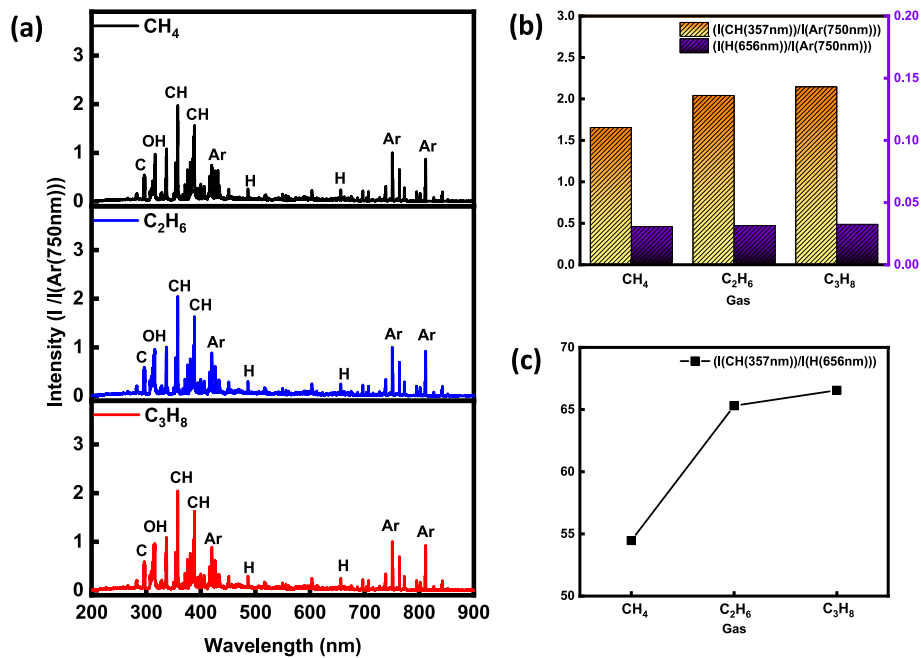


Fig. 6. (a) OES data for C_xH_{2x+2} ($x = 1, 2, 3$) mixed with 50% Ar. (b) The ratios of CH/Ar and H/Ar, and (c) the ratio of CH/H for different C_xH_{2x+2} ($x = 1, 2, 3$).

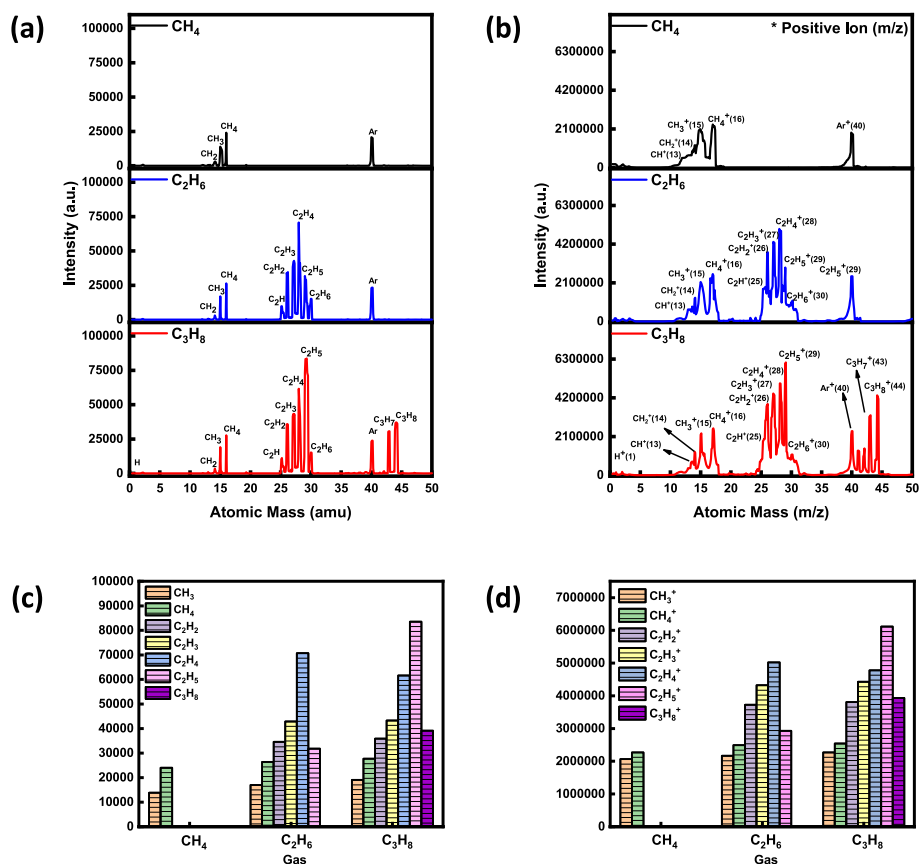
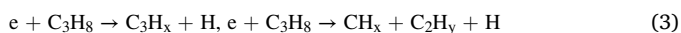
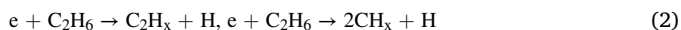


Fig. 7. QMS data of (a) and (c) radical mode, and (b) and (d) positive ion mode for C_xH_{2x+2} ($x = 1, 2, 3$) mixed with 50% Ar.

plasma can be estimated by the positive ion mode. However, as shown in Fig. 7 (a) and (b), no significant differences in dissociated species could be observed between the dissociated species in the plasma estimated by the radical mode and positive ion mode for C_xH_{2x+2} ($x = 1, 2, 3$), indicating no significant fragmentation of species in the QMS for the radical mode. As shown in Fig. 7 (a)–(d), higher mass species were observed for C_2H_6 compared to CH_4 by showing C_2H_x ($x=(1-6)$), in addition to CH_x ($x=(1-4)$), and, for C_3H_8 , also by showing C_3H_x ($x=(4-8)$), in addition to C_2H_x ($x=(1-6)$) and CH_x ($x=(1-4)$), while showing no significant hydrogen peak, such as H or H_2 , for all the C_xH_{2x+2} ($x = 1, 2, 3$). Therefore, from the observed data from OES and QMS, it is believed that C_xH_y ($y > x$, $y/x = (1-3)$) appears to be important in the etching of ITO through the following dissociation of hydrocarbon gases of Eqs. (1)–(3) in the plasma:



The radicals and ions dissociated from C_xH_{2x+2} ($x = 1, 2, 3$) arrive at the substrate, and form compounds with ITO, and the reacted compounds are removed from the ITO surface by sputtering by ion bombardment, such as Ar^+ ions. The ITO surface composition before the etching (reference) and during the etching using C_xH_{2x+2} ($x = 1, 2, 3$) mixed with 50% Ar was measured using XPS, and the results are shown in Fig. 8, which shows that the etching using CH_x decreased Sn content on the surface, possibly due to the preferential removal of Sn from the ITO by the formation of SnH_x (boiling point of SnH_4 is $-52^\circ C$). By using the hydrocarbon gas with higher C/H ratio, the indium percentage was decreased with the increase of carbon percentage and the decrease of the oxygen percentage, indicating formation of a hydrocarbon polymer

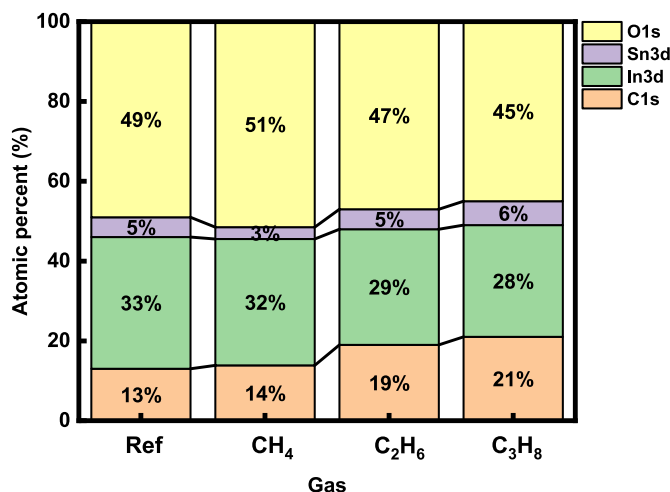


Fig. 8. Atomic percentages of ITO surface before and after the ITO etching with C_xH_{2x+2} ($x = 1, 2, 3$) mixed with 50% Ar measured by XPS.

layer on the ITO surface, and the removal of In from the surface by the formation of indium hydrocarbon compounds, such as InC_xH_y ($x < y$, $y/x = (1-3)$) (boiling point of $In(CH_3)_{2-3}$ is $136^\circ C$) and through the sputtering of the compounds by ion bombardment, such as Ar^+ ion, due to the low volatility. In the case of Sn, the surface composition was similar to the reference with the hydrocarbon gas with higher C/H ratios; therefore, Sn appears to be more preferentially removed by the formation of SnH_x , rather than the formation of Tin hydrocarbon compounds, such as SnC_xH_y ($x < y$, $y/x = (1-3)$) (the boiling point of $Sn(CH_3)_3$ is $58^\circ C$).

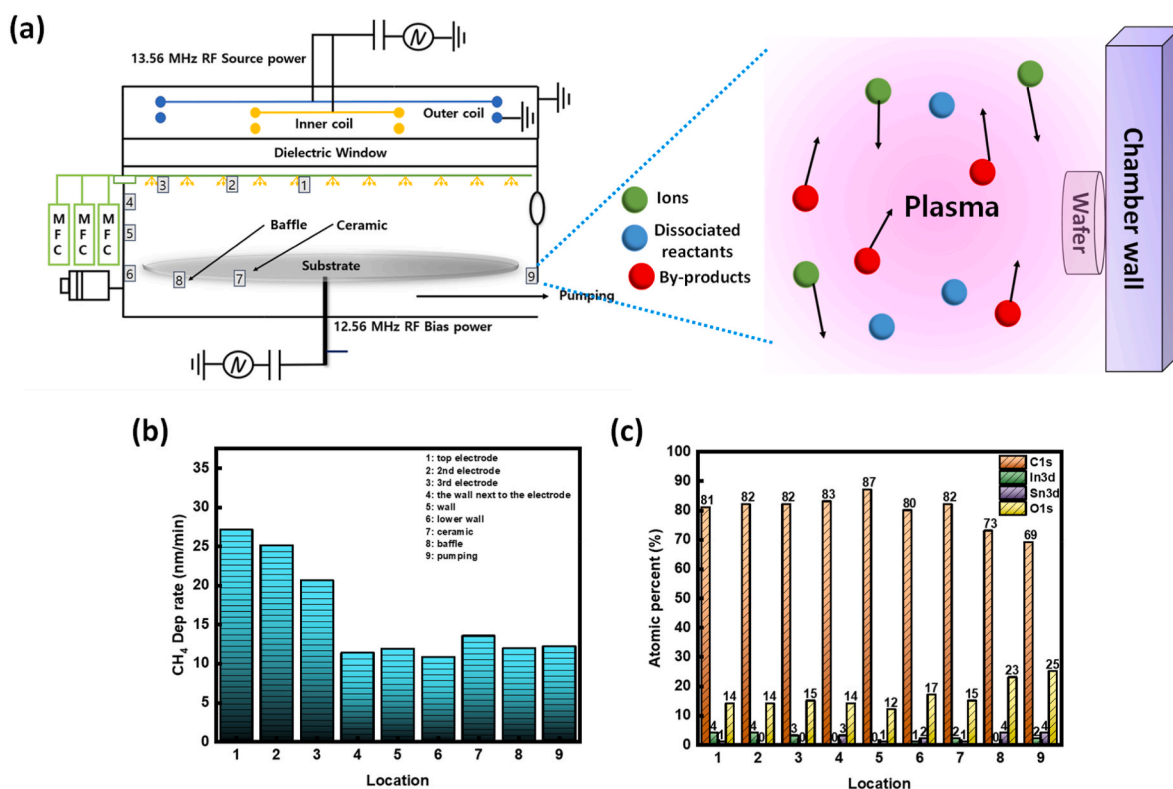


Fig. 9. (a) Schematic showing the location of silicon wafers attached to the chamber wall. (b) The etch byproduct deposition rate as a function of chamber location during the ITO etching. (c) Composition of the residue measured by XPS. The etch residue was observed after the etching of 1 μm thick blank ITO covering the substrate holder with the etch conditions of CH₄/50% Ar in Fig. 3.

3.2. Thickness and composition of etch residue deposited on the chamber wall

The hydrocarbon compounds of In and Sn formed on the ITO surface

can be sputter etched from the ITO surface and deposited on the chamber wall, due to the low volatility of the compounds. Fig. 9 shows (b) the deposition rate, and (c) the composition of the etch residue deposited (a) on the various chamber wall locations during the ITO

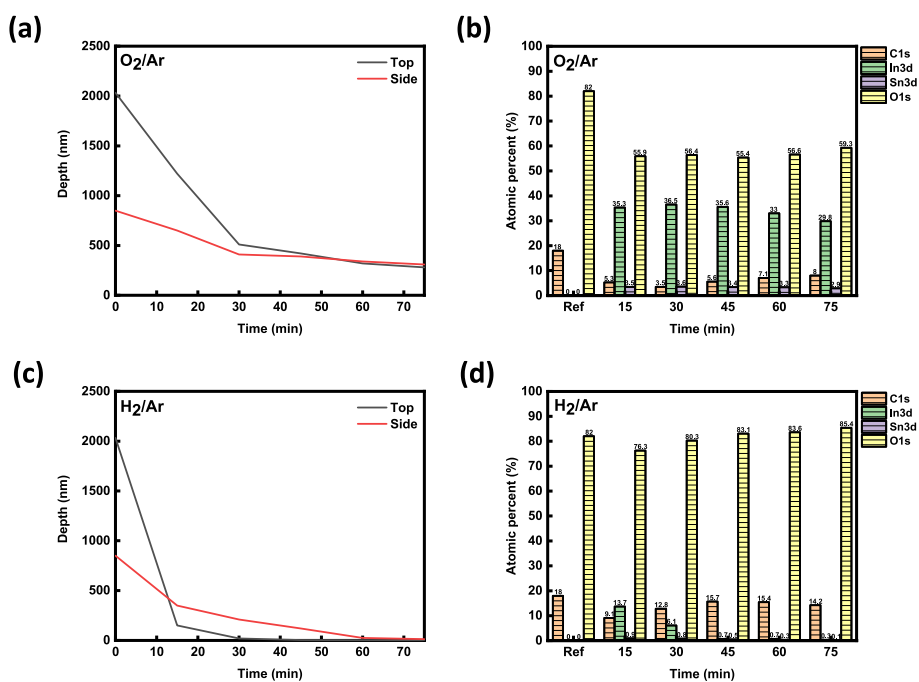


Fig. 10. Cleaning of etch residue on the chamber wall at locations 1 (the highest residue deposition rate position) and 6 (the lowest residue deposition rate position), with (a) O₂/Ar (1:5) plasma, and (c) H₂/Ar (1:1) plasma, measured by cleaning time. Composition of the remaining residue at location 1 measured by XPS as a function of cleaning time for the cleaning with (b) O₂/Ar plasma, and (d) H₂/Ar plasma.

etching, using the CH_4/Ar with the etch conditions in Fig. 3. To observe the etch residue on the chamber wall, ITO glass substrate covering the 300 mm diameter substrate holder was used, and the etch residue was measured after the etching of 1 μm thick ITO, that is, for 75 min. To measure the etch residue deposition rate along the various locations of the chamber wall, 9 silicon wafers were attached equally by covering the chamber top position, chamber sidewall area, and pumping area, as shown in Fig. 9 (a). Fig. 9 (b) shows that the highest deposition rate of etch residue was observed at the chamber top area, because the chamber top area faces the ITO surface during the etching, while the lowest deposition rate was observed at the chamber sidewall area, possibly due to the separation from the plasma area. The residue was composed of mostly hydrocarbon, as shown in Fig. 9 (c), and the highest indium content was observed in the hydrocarbon layer at the chamber top area, while the lowest indium content was observed at the chamber wall side, while both indium and tin residues were observed at the pumping area.

3.3. Cleaning of etch residue deposited on the chamber wall using H_2/Ar plasma

The etch residue formed on the wall of the chamber after 1 μm thick ITO etching for 75 min with the etch conditions of CH_4/Ar in Fig. 3 was cleaned by using the ICP source plasma only, without biasing the substrate. Fig. 10 shows the remaining residue thickness and composition of the remaining residue measured as a function of cleaning time with (a) and (b) 1:5 ratio of O_2/Ar , and (c) and (d) 1:1 ratio of H_2/Ar . The ICP source power of 2000 W and 30 mTorr of operating pressure were used for etch residue cleaning. As shown in Fig. 10 (a), when O_2/Ar plasma was used to clean the etch residue formed on the chamber wall, even though the residue was partially cleaned by the plasma initially until 30 min cleaning, ~ 400 nm thick residue was remaining, both in the chamber top area and chamber wall area, and the further cleaning time did not decrease the remaining residue thickness. When the composition of the remaining residue was measured by XPS, as shown in Fig. 10 (b), nonvolatile indium oxide and tin oxide appeared to be remaining on the chamber wall after the removal of the hydrocarbon of residue by forming CO_x and H_2 . However, as shown in Fig. 10 (c), when H_2/Ar was used for the residue cleaning, the residue on the chamber top area appears to be cleaned completely after ~ 30 min cleaning, while the residue on the chamber sidewall area appears to be cleaned after ~ 65 min. Fig. 10 (d) shows that for the chamber top location, most of the indium (and also tin) was removed after 30 min cleaning with H_2/Ar plasma, possibly in the form of InC_xH_y (and SnH_x), in addition to the cleaning of hydrocarbon layer by CH_x with the assistance of low-energy Ar^+ ion bombardment. For the cleaning, the use of higher operating pressure up to 90 mTorr increased the cleaning rate at the top position (shown in Fig. S3 of the SI). For the H_2/Ar gas mixture ratio from (2:1 to 1:2), the H_2/Ar ratio of 1:1 appears to show the highest residue removal rate (shown in Fig. S4 of the SI).

The thickness of etch residue deposited during the etching of 1 μm thick ITO with the etch conditions in Fig. 3 and the time required to clean the deposited residue formed on the chamber wall with the cleaning conditions of H_2/Ar in Fig. 10 were investigated for all three $\text{C}_x\text{H}_{2x+2}$ ($x = 1, 2, 3$) gases, and the results are shown in Fig. 11 for (a) chamber top position 1, and (b) chamber sidewall position 6. To measure the deposited residue thickness and the remaining residue thickness, silicon wafers were attached to the top position 1 and chamber sidewall position 6, and the residue thickness on the silicon wafers was measured during the deposition and cleaning. As shown in Fig. 11 (a) and (b), the use of hydrocarbon gas of $\text{C}_x\text{H}_{2x+2}$ ($x = 1, 2, 3$) with higher C/H ratio decreased ITO etch time due to the higher ITO etch rate, and lowered the deposited thickness of the residue on the chamber wall for the etching of the same 1 μm thick ITO. The cleaning time required to remove the remaining etch residue thickness appears to be similar for all three hydrocarbon gases, or a little longer for the hydrocarbon gas with higher C/H ratio. Therefore, the total time required to etch 1 μm thick ITO and to fully clean the chamber wall area was shorter in the order: CH_4 (160 min) < C_2H_6 (145 min) < C_3H_8 (135 min). Therefore, the total ITO etch processing time can be improved by using the novel hydrocarbon gases with higher C/H ratio, such as C_2H_6 and C_3H_8 , in addition to the improvement of the ITO etch characteristics, such as the etch selectivity over PR, etch profile, etc. *In situ* deposition and cleaning of etch residue at the sidewall of the chamber was also measured by using QCM, and the results are similar to the those in Fig. 11, as shown in Fig. S5 of the SI, in which the compositional changes of the residue with cleaning time at the top position 1 and sidewall position 6 are also shown for three different hydrocarbon gas of $\text{C}_x\text{H}_{2x+2}$ ($x = 1, 2, 3$), and no significant differences in the composition as a function of cleaning time could be observed.

3.4. ITO etching and etch residue removal mechanisms

From the above observations, the ITO etch mechanism by $\text{C}_x\text{H}_{2x+2}$ ($x = 1, 2, 3$) mixed with Ar and the residue cleaning mechanism by H_2/Ar plasma can be estimated, as shown in Fig. 12. During ITO etching, the dissociated C_xH_y ($x < y, y/z = (1-3)$) and H and the reactive ions, such as C_xH_y^+ ($x < y, y/z = (1-3)$) and H^+ , are chemisorbed on the ITO, and form compounds, such as InC_xH_y , SnH_x (SnC_xH_y), and C_xH_y . The chemisorbed species on ITO surfaces are loosely bound to the ITO; therefore, they are simultaneously sputtered off from the surface of ITO by Ar^+ ion impingement while etching using $\text{C}_x\text{H}_{2x+2}$ ($x = 1, 2, 3$) mixed with Ar. Even though compounds such as SnH_4 and CO_x ($x = 1, 2$) can be removed to the pump by the high vapor pressure, the compound species, such as InC_xH_y and SnC_xH_y (and SnH_x ($x=(1-3)$)) are sticky and have less volatility; therefore, they can be accumulated on the chamber wall, and form a polymer etch residue with the C_xH_y radicals in the plasma attached to the chamber wall during the etching.

Using the H_2/Ar plasma, the etch residue composed of a

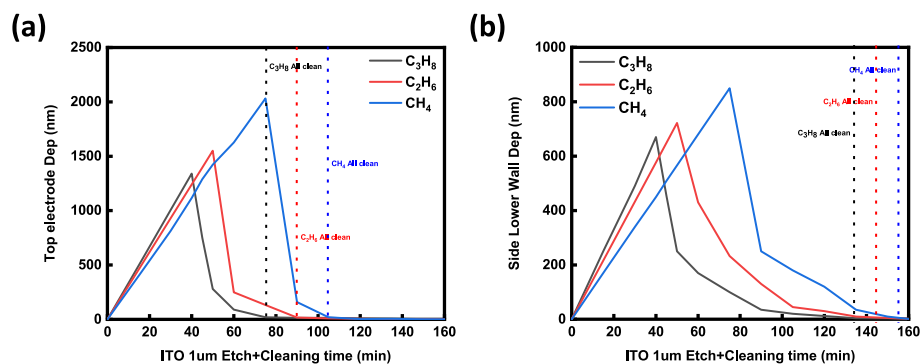


Fig. 11. Thickness of etch residue deposited during the etching of 1 μm thick ITO with $\text{C}_x\text{H}_{2x+2}$ ($x = 1, 2, 3$)/Ar with the conditions in Fig. 3 and following cleaning with H_2/Ar plasma in Fig. 10 for (a) chamber top position 1, and (b) chamber sidewall position 6.

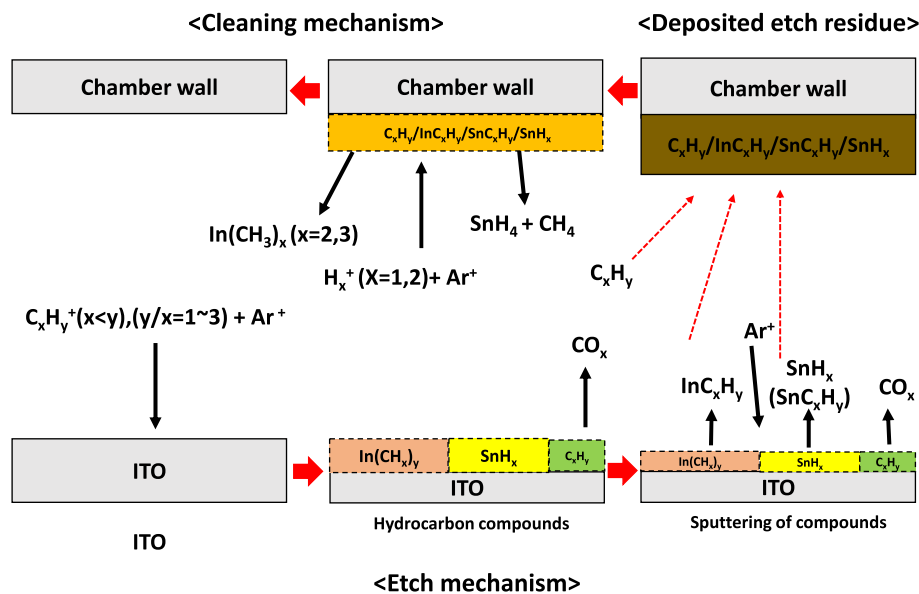


Fig. 12. Schematic of the possible ITO etch and cleaning mechanism for the etching with C_xH_{2x+2} ($x = 1, 2, 3$) and cleaning with H_2/Ar .

hydrocarbon polymer layer, InC_xH_y , and SnC_xH_y (and SnH_x ($x=(1-3)$)) appears to be cleaned first by forming more volatile SnH_4 and CH_4 ; and after that, by forming more volatile metal organic indium molecules, such as $In(CH_3)_x$, through the assistance of low-energy Ar^+ ion bombardment.

4. Conclusions

In this study, the etch characteristics of ITO by using hydrocarbon gases with alkane structure of C_xH_{2x+2} mixed with Ar, including novel etch gases, such as ethane (C_2H_6) and propane (C_3H_8), and the etch residue cleaning characteristics with H_2/Ar were investigated. The use of C_xH_{2x+2} with higher C/H ratio both improved the ITO etch rate and increased the etch selectivity over PR due to the decreased hydrogen in the gas mixture, which not only increases PR etching, but also damages the PR. Therefore, smoother and more anisotropic ITO etching could be obtained in the order $CH_4 > C_2H_6 > C_3H_8$. The ITO etching by the C_xH_{2x+2} mixed with Ar is due to the compound formation (ex, InC_xH_y , SnH_x , and SnC_xH_y (and C_xH_y)) on the ITO surface after the removal of O by CO_x and the sputtering of these compounds by Ar^+ ion bombardment. Among the sputtered compounds, less volatile and less sticky compounds, such as InC_xH_y and SnC_xH_y , in addition to C_xH_y from the plasma, are attached to the chamber wall, and form a polymer etch residue layer. This polymer layer formed by C_xH_{2x+2} could be successfully removed with H_2/Ar plasma by forming more volatile compounds, such as $In(CH_3)_x$, SiH_4 , and CH_4 . It is believed that the hydrocarbon with higher C/H ratio, such as C_3H_8 , will be applicable to the fabrication of the next generation display device, due to the excellent etch characteristics, such as higher etch rate, higher etch selectivity over PR, smoother and more anisotropic etch profiles, easy removal of etch residue on the chamber wall, etc.

CRediT authorship contribution statement

Jong Woo Hong: Writing – review & editing, Writing – original draft. **Hyun Min Cho:** Data curation. **Yu Gwang Jeong:** Supervision. **Da Woon Jung:** Investigation. **Yun Jong Yeo:** Data curation. **Ji Eun Kang:** Data curation. **Hee Ju Kim:** Data curation. **Hyun Woo Tak:** Resources. **Geun Young Yeom:** Formal analysis, Data curation. **Dong Woo Kim:** Data curation.

Declaration of competing interest

The authors declare that they have no known competing financial interests or personal relationships that could have appeared to influence the work reported in this paper.

Data availability

Data will be made available on request.

Acknowledgments

This work was supported by Samsung Display Co., Ltd., the Korea Institute of Energy Technology Evaluation and Planning (KETEP), the Ministry of Trade, Industry & Energy (MOTIE) of the Republic of Korea (No. 20202010100020), the Ministry of Trade, Industry & Energy (MOTIE) (1415179251), and the Korea Semiconductor Research Consortium (KSRC) (20011977) support program for the development of the future semiconductor device.

Appendix A. Supplementary data

Supplementary data to this article can be found online at <https://doi.org/10.1016/j.mssp.2023.107395>.

References

- [1] L. Wen, B.B. Sahu, G.Y. Yeom, J.G. Han, Room temperature deposition of very thin and flexible crystalline ITO thin film using 3-D facing-magnetron sputtering plasma source, *Vacuum* 193 (2021), <https://doi.org/10.1016/j.vacuum.2021.110520>.
- [2] L. Wen, B.-B. Sahu, J.-G. Han, G.-Y. Yeom, Improved electrical and optical properties of ultra-thin tin doped indium oxide (ITO) thin films by a 3-dimensionally confined magnetron sputtering source, *Sci. Adv. Mater.* 13 (2021) 1498–1505, <https://doi.org/10.1166/sam.2021.4020>.
- [3] O.A. Ghandour, D. Constantinide, R. Sheets, Excimer Ablation of ITO on Flexible Substrates for Large Format Display Applications, 2002, in: <http://proceedings.spiedigitallibrary.org/>.
- [4] D.S. Leem, T. Lee, T.Y. Seong, Enhancement of the light output of GaN-based light-emitting diodes with surface-patterned ITO electrodes by maskless wet-etching, *Solid State Electron.* 51 (2007) 793–796, <https://doi.org/10.1016/j.sse.2007.02.038>.
- [5] J.H. Jang, M.C. Oh, Outcoupling enhancement of OLEDs with a randomly distributed ITO pattern fabricated by maskless wet etching method, *IEEE/OSA Journal of Display Technology* 9 (2013) 900, <https://doi.org/10.1109/JDT.2013.2265696>. –903.

- [6] T.H. Tsai, Y.F. Wu, Wet etching mechanisms of ITO films in oxalic acid, *Microelectron. Eng.* 83 (2006) 536–541, <https://doi.org/10.1016/j.mee.2005.12.003>.
- [7] C.J. Huang, Y.K. Su, S.L. Wu, The effect of solvent on the etching of ITO electrode, *Mater. Chem. Phys.* 84 (2004) 146–150, <https://doi.org/10.1016/j.matchemphys.2003.11.021>.
- [8] C.J. Lee, H.K. Lin, C.H. Li, L.X. Chen, C.C. Lee, C.W. Wu, J.C. Huang, A study on electric properties for pulse laser annealing of ITO film after wet etching, in: *Thin Solid Films*, 2012, pp. 330–335, <https://doi.org/10.1016/j.tsf.2012.09.010>.
- [9] T.-H. Tsai, Y.-F. Wu, Organic acid mixing to improve ITO film etching in flat panel display manufacturing, *J. Electrochem. Soc.* 153 (2006) C86, <https://doi.org/10.1149/1.2135221>.
- [10] Y.J. Lee, J.W. Bae, H.R. Han, J.S. Kim, G.Y. Yeom, *Dry Etching Characteristics of ITO Thin Films Deposited on Plastic Substrates*, 2001.
- [11] J.Y. Park, H.S. Kim, D.H. Lee, K.H. Kwon, G.Y. Yeom, *A Study on the Etch Characteristics of ITO Thin Film Using Inductively Coupled Plasmas*, 2000.
- [12] J.Y. Park, H.S. Kim, D.H. Lee, K.H. Kwon, G.Y. Yeom, *A Study on the Etch Characteristics of ITO Thin Film Using Inductively Coupled Plasmas*, 2000.
- [13] R. Fang, W.J. Jiang, X. Guo, J.R. Han, G. di Shen, A study on the Cl₂/C₂H₄/Ar plasma etching of ITO using inductively coupled plasma, in: *Optoelectronic Materials and Devices IV*, SPIE, 2009, p. 76310S, <https://doi.org/10.1117/12.850056>.
- [14] Y.H. Joo, J.C. Woo, K.R. Choi, H.S. Kim, J.H. Wi, C. il Kim, Dry etching of ITO thin films by the addition of gases in Cl₂/BCl₃ inductivity coupled plasma, *Transactions on Electrical and Electronic Materials* 13 (2012) 157–161, <https://doi.org/10.4313/TEEM.2012.13.3.157>.
- [15] H.W. Yoon, S.M. Shin, S.Y. Kwon, H.M. Cho, S.G. Kim, M.P. Hong, One-step etching characteristics of ito/ag/ito multilayered electrode in high-density and high-electron-temperature plasma, *Materials* 14 (2021), <https://doi.org/10.3390/ma14082025>.
- [16] D.Y. Kim, J.H. Ko, M.S. Park, N.E. Lee, Infinitely high etch selectivity during CH₄/H₂/Ar inductively coupled plasma (ICP) etching of indium tin oxide (ITO) with photoresist mask, *Thin Solid Films* 516 (2008) 3512–3516, <https://doi.org/10.1016/j.tsf.2007.08.021>.
- [17] A. Hirata, M. Fukasawa, K. Kugimiya, K. Karahashi, S. Hamaguchi, K. Nagaoka, Damage recovery and low-damage etching of ITO in H₂/CO plasma: effects of hydrogen or oxygen, *Plasma Process. Polym.* 16 (2019), <https://doi.org/10.1002/ppap.201900029>.
- [18] A. Hirata, M. Fukasawa, T. Shigetoshi, M. Okamoto, K. Nagahata, H. Li, K. Karahashi, S. Hamaguchi, T. Tatsumi, Effects of hydrogen-damaged layer on tin-doped indium oxide etching by H₂/Ar plasma, in: *Jpn J Appl Phys*, Japan Society of Applied Physics, 2017, <https://doi.org/10.7567/JJAP.56.06HD02>.
- [19] S.A. Vitale, S. Berry, Etching selectivity of indium tin oxide to photoresist in high density chlorine- and ethylene-containing plasmas, *Journal of Vacuum Science & Technology B, Nanotechnology and Microelectronics: Materials, Processing, Measurement, and Phenomena* 31 (2013), 021210, <https://doi.org/10.1116/1.4795209>.
- [20] G. Cunge, B. Pelissier, O. Joubert, R. Ramos, C. Maurice, New chamber walls conditioning and cleaning strategies to improve the stability of plasma processes, *Plasma Sources Sci. Technol.* 14 (2005) 599–609, <https://doi.org/10.1088/0963-0252/14/3/025>.
- [21] K. Raiber, A. Terfort, C. Benndorf, N. Krings, H.H. Strehblow, Removal of self-assembled monolayers of alkanethiolates on gold by plasma cleaning, *Surf. Sci.* 595 (2005) 56–63, <https://doi.org/10.1016/j.susc.2005.07.038>.
- [22] W. Petasch, B. Kegel, H. Schmid, K. Lendenmann, H.U. Keller, *Low-pressure Plasma Cleaning: a Process for Precision Cleaning Applications*, 1997.
- [23] K.J. Clay, S.P. Speakman, G.A.J. Amaratunga, S.R.P. Silva, Characterization of a-C:H:N deposition from CH₄/N₂ rf plasmas using optical emission spectroscopy, *J. Appl. Phys.* 79 (1996) 7227–7233, <https://doi.org/10.1063/1.361439>.
- [24] P. Attri, T. Sarinont, M. Kim, T. Amano, K. Koga, A.E. Cho, E.H. Choi, M. Shiratani, Influence of ionic liquid and ionic salt on protein against the reactive species generated using dielectric barrier discharge plasma, *Sci. Rep.* 5 (2015), <https://doi.org/10.1038/srep17781>.
- [25] H.W. Tak, H.J. Lee, L. Wen, B.J. Kang, D. Sung, J.W. Bae, D.W. Kim, W. Lee, S. B. Lee, K. Kim, B.O. Cho, Y.L. Kim, H.D. Song, G.Y. Yeom, Effect of hydrofluorocarbon structure of C₃H₂F₆ isomers on high aspect ratio etching of silicon oxide, *Appl. Surf. Sci.* 600 (2022), <https://doi.org/10.1016/j.apsusc.2022.154050>.